Analytical approach for the design of cascaded raman fiber lasers

A. Martínez Rios, I. Torres Gómez, R. Selvas Aguilar, G. Anzueto Sanchez, and A.N. Starodumov*
Centro de Investigaciones en Óptica, A.C.,
León, Guanajuato, México, 37150
e-mail: amr6@cio.mx

Recibido el 6 de diciembre de 2004; aceptado el 28 de abril de 2005

An analytical approach for the design of cascaded Raman fiber lasers is presented. The model computes the values of the pump and Stokes powers at the fiber laser output based on the boundary conditions, the invariants resultanting from the analysis of the coupled differential equations, and assuming that the sum of the forward and backward Stokes waves resonated inside the cavity is constant. The model is applied to Raman fiber lasers based on five nested cavities and compared with published results based on numerical models obtaining a good correlation.

Keywords: Optical fibers; fiber lasers; cascaded raman fiber lasers; modeling.

Presentamos una aproximación analítica para el diseño de láseres Raman de fibra óptica con configuración en cascada. El modelo calcula los valores de las potencias de las ondas de bombeo y ondas Stokes en el extremo de salida del láser de fibra usando las condiciones en la frontera, las invariantes resultantes del análisis del sistema de ecuaciones acopladas, y suponiendo que la suma de las ondas Stokes resonadas dentro de la cavidad es constante. El modelo se utiliza para analizar el caso de un láser Raman de fibra óptica con cinco cavidades anidadas, y los resultados, se comparan con los obtenidos mediante métodos numéricos en la literatura logrando una buena correlación.

Descriptores: Fibras ópticas; láseres de fibra; láseres Raman en cascada: modelado.

PACS: 42.55.Wd; 42.55.Ye

1. Introduction

Raman Stokes generation in silica-based fibers is now an established technique for the generation of laser light in the transparency range of optical fibers, particularly in the wavelength range of 1.1-1.9μm. Nested [1], chained [2], ring [3], and composite [4] cavities have been used for the generation of cascade Stokes waves with multiple output wavelengths. Most of these sources are thought to be used as pump sources for discrete and distributed Raman amplifications, as well as remote pumping of Er^{3+}-doped fiber amplifiers, in long-haul telecommunication fiber systems. The multiple output Stokes wavelengths are generated among the Raman gain bands of the optical fiber, and they are selected to provide flat and broad gain over the optical band of interest (S^+-band, S-band, M-band, L-band, and/or L^+-band). Several numerical models for single [5-8] and multiple [9] output wavelengths cascaded Raman lasers have been published. Analytical models have also been published for single cavity Raman lasers [10], and single wavelength cascaded Raman fiber lasers [11]. In contrast with the numerical modeling of Raman fiber lasers, which obscures the physics of the process, analytical models permit a better understanding of the parameters affecting the fiber performance through a simple inspection of the solutions. In this paper, we use an analytical approach for the solution of the coupled power equations that describe the interactions and performance of cascaded Raman fiber lasers.

2. Model

Figure 1 shows a schematic diagram of a Raman fiber laser with five nested cavities, consisting of high reflection fiber Bragg gratings spliced on both ends of the GeO_2-doped silica fiber. Coupled power equations describing the interaction among n-Stokes waves inside the nested cavities are expressed as [7]:

$$\frac{dP_n^{\pm}(z)}{dz} = \left[\mp\frac{\lambda_{n+1}}{\lambda_n} g_{n,n+1}\left(P_{n+1}^{+}(z) + P_{n+1}^{-}(z)\right) \pm g_{n-1,n}\left(P_{n-1}^{+}(z) + P_{n-1}^{-}(z)\right) - \alpha_n\right] P_n^{\pm}(z), \quad (1)$$

where $P_n^{\pm}(z)$ is the power of the nth-Stokes wave propagating in the forward or backward direction, α_n is the loss coefficient at the wavelength of the nth Stokes wave, and the Raman gain $g_{n,n+1}$ is defined by

$$g_{n,n+1} = \frac{g_R/\lambda_n(\mu m)}{A_{n,n+1}}, \quad (2)$$

where g_R is the Raman gain coefficient, λ_n is the wavelength of the n pump wave for the n+1 Stokes wave, and $A_{n,n+1}$ is the effective interaction area between the pump and Stokes waves. The effective interaction area is related to the mode field radii W_n through [12]:

$$A_{n,n+1} = \frac{\pi}{2}\left(W_n^2 + W_{n+1}^2\right). \quad (3)$$

From relation (1), we can obtain the following constant independent of distance z [10]:

$$K_n = P_n^{+}(z)P_n^{-}(z) \quad (4)$$

We will consider the following boundary conditions for the resonated waves:

$$P_n^{+}(z_n^m) = R_n P_n^{-}(z_n^m) \quad (5)$$

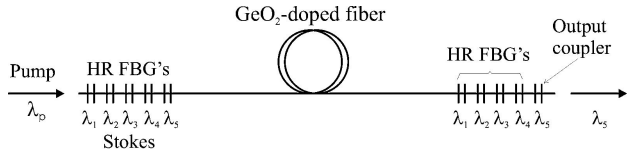

FIGURE 1. Schematic diagram of a five-nested cavities Raman fiber laser.

$$P_n^-(z_n^{out}) = R'_n P_n^+(z_n^{out}), \tag{6}$$

where R_n and R'_n are the mirror reflectivities at the input and output side of the nth-cavity, respectively. The length of the nth-cavity is given by $L_n = z_n^{out} - z_n^{in}$, where the notation accounts for the possibility of chained or composite cavities. In the case of a nested cavity fiber Raman laser, we will have $z_n^{in} = 0$ y $z_n^{out} = L$. We will assume that $n = 0$ stands for the pump wave that is not resonated.

The general solution of Eq. (1) is given by

$$P_n^{\pm}(z)=P_n^{\pm}(z_n^{in})\exp\left[\mp\frac{\lambda_{n+1}}{\lambda_n}g_{n,n+1}\int_{z_n^{in}}^{z}\left(P_{n+1}^{+}+P_{n+1}^{-}\right)dz \pm g_{n-1,n}\int_{z_n^{in}}^{z}\left(P_{n-1}^{+}+P_{n-1}^{-}\right)dz-\alpha_n\left(z-z_n^{in}\right)\right]. \tag{7}$$

For the resonated Stokes waves we have the following oscillation condition

$$-\frac{\lambda_{n+1}}{\lambda_n}g_{n,n+1}\int_{z_n^{in}}^{z_n^{out}}\left(P_{n+1}^{+}+P_{n+1}^{-}\right)dz + g_{n-1,n}\int_{z_n^{in}}^{z_n^{out}}\left(P_{n-1}^{+}+P_{n-1}^{-}\right)dz = -\frac{1}{2}\ln\left(R_n^{in}R_n^{out}\right)+\alpha_n L_n, \tag{8}$$

where it is assumed that all the resonated Stokes waves are over the laser threshold.

The main assumption of our model is that the sum of the forward and backward resonated waves is approximately constant for all the resonated Stokes waves. This assumption was already used in Ref. 13 to obtain an analytical model for two cascades Raman fiber laser. In addition, we assume that the pump wave suffers strong depletion, so that we may approximate the integral over the cavity length L of sum of the forward and backward pump waves as follows:

$$\int_0^L (P_0^+ + P_0^-)dz \approx \frac{P_0^+(0)}{\frac{\lambda_1}{\lambda_0}g_0(P_1^+ + P_1^-)+\alpha_0}. \tag{9}$$

Under the assumption of a small-signal regime for the last Stokes wave that is not resonated, we found that the integral over L of the sum of the forward and backward portions of such wave may be approximated as

$$\int_0^L (P_n^+ + P_n^-)dz \approx \frac{2P_n^+(0)}{g_{n-1}(P_{n-1}^+ + P_{n-1}^-)-\alpha_n} \times \sinh[g_{n-1}(P_{n-1}^+ + P_{n-1}^-)-\alpha_n]. \tag{10}$$

Relations (9) and (10) are useful to link the complete set of equations arising from the resonance condition [Eq. (8)] for each laser wavelength. In order to simplify as much as possible the analytical solution, we only use Eq. (10) as an accessory condition, so that after obtaining adequate relations we assume that $P_m \approx 0$ (where m corresponds to the Stokes wave following the last resonated Stokes wave, *i.e.*, m=n+1).

From Eqs. (8) to(10), using the last approximations and rearranging, we obtain the following set of coupled equations,

$$\left(-\frac{\lambda_2}{\lambda_1}g_1\left(P_2^+ + P_2^-\right)L-\alpha_1 L+\frac{1}{2}\ln\left(R_1R'_1\right)\right)\left(\frac{\lambda_1}{\lambda_0}g_0(P_1^+ + P_1^-)+\alpha_0\right)+g_0P_0^+ = 0. \tag{11}$$

$$-\tfrac{\lambda_3}{\lambda_2}g_2\left(P_3^+ + P_3^-\right)L + g_1(P_1^+ + P_1^-)L-\alpha_2 L+\tfrac{1}{2}\ln\left(R_2R'_2\right)=0.$$

$$\vdots \tag{12}$$

$$-\tfrac{\lambda_{n-1}}{\lambda_{n-2}}g_{n-2}\left(P_{n-1}^+ + P_{n-1}^-\right)L + g_{n-3}(P_{n-3}^+ + P_{n-3}^-)L-\alpha_{n-2}L+\tfrac{1}{2}\ln\left(R_{n-2}R'_{n-2}\right)=0.$$

$$\left(g_{n-2}\left(P_{n-2}^+ + P_{n-2}^-\right)L-\alpha_{n-1}L+\frac{1}{2}\ln\left(R_{n-1}R'_{n-1}\right)\right)\left(g_{n-1}(P_{n-1}^+ + P_{n-1}^-)-\alpha_n\right)=0. \tag{13}$$

Relations (11) to (13) can be easily modified taking into account different cavity lengths. By using,

$$P_{n-1}^+(L) + P_{n-1}^-(L) = P_{n-1}^+(L)(1+R'_{n-1}), \tag{14}$$

and

$$P_{n-1}^{transmitted} = P_{n-1}^+(L)(1-R'_{n-1}) \tag{15}$$

we found that the transmitted power for 1-cavity, 2-cavities, 3-cavities, and 5-cavities Raman lasers can be written as:

$$P_{out}^{1-cav} = \frac{\lambda_0}{\lambda_1}\frac{(1-R_1')}{(1+R_1')}\left(-\frac{P_0^+(0)}{(1/2)\ln(R_1R_1')-\alpha_1 L}-\frac{\alpha_0}{g_0}\right). \tag{16}$$

$$P_{out}^{2-cav} = \frac{\lambda_1}{\lambda_2}\frac{(1-R_2')}{(1+R_2')}\left(\frac{g_0}{g_1}\frac{P_0^+(0)}{(\lambda_1 g_0/\lambda_0 g_1)[\alpha_2 L-(1/2)\ln(R_2R_2')]+\alpha_0 L}+\frac{\ln(R_1)}{g_1 L}-\frac{\alpha_1}{g_1}\right). \tag{17}$$

$$P_{out}^{3-cav} = \frac{\lambda_2}{\lambda_3}\frac{(1-R_3')}{(1+R_3')}\left(\frac{\lambda_0 g_1}{\lambda_1 g_2}\frac{P_0^+(0)}{(\lambda_2 g_1/\lambda_1 g_2)[\alpha_3 L-(1/2)\ \ln(R_3R_3')]-\ln(R_1)+\alpha_1 L}+\frac{\ln(R_2)-\alpha_2 L}{g_2 L}-\frac{\lambda_0 g_1\alpha_1}{\lambda_1 g_0 g_2}\right). \tag{18}$$

$$\begin{aligned}P_{out}^{5-cav} = {}& \frac{\lambda_4}{\lambda_5}\frac{(1-R_5')}{(1+R_5')}\left\{-\frac{\lambda_0\lambda_2 g_1 g_3\alpha_0}{\lambda_1\lambda_3 g_0 g_2 g_4}-\frac{\lambda_2 g_3\alpha_2}{\lambda_3 g_2 g_4}-\frac{\alpha_4}{\lambda_1 g_4}+\frac{1}{2}\frac{\lambda_2 g_3\ln(R_2R_2')}{\lambda_3 g_2 g_4 L}+\frac{1}{2}\frac{\ln(R_4R_4')}{g_4 L}\right.\\ &\times P_0^+(0)/\left(\frac{1}{2}\frac{\lambda_2\lambda_3 g_2 g_4\alpha_1 L}{\lambda_0\lambda_2 g_1 g_3}+\frac{1}{2}\frac{\lambda_3 g_4\alpha_3 L}{\lambda_0 g_3}+\frac{1}{2}\frac{\lambda_4}{\lambda_0}\alpha_5 L-\frac{1}{4}\frac{\lambda_1\lambda_3 g_2 g_4\ln(R_1R_1')}{\lambda_0\lambda_2 g_1 g_3}\right.\\ &\left.\left.-\frac{1}{4}\frac{\lambda_3 g_4\ln(R_3R_3')}{\lambda_0 g_3}-\frac{1}{4}\frac{\lambda_4\ln(R_5R_5')}{\lambda_0}\right)\right\}.\end{aligned} \tag{19}$$

Relations (17) to (19) show the dependence of the Raman fiber laser output on the parameters of the cavities, *i.e.*, pump power, Raman gain, mirror reflectivities, wavelengths, loss, and fiber length. The model neither includes the effect of amplified spontaneous emission nor Rayleigh backscattering that affect the effective power transfer among successive Stokes waves.

3. Raman gain

The peak Raman gain for pure silica at frequency shift 13.2 THz is estimated from the following relation [14]:

$$g_R(\mathrm{SiO_2}) = 0.99\times 10^{-13}/\lambda\ [m/W], \tag{20}$$

where λ is in μm. For random or depolarized pump evolution, the Raman gain coefficient must be reduced by a factor of 2. Pure GeO_2 has a peak Raman gain coefficient at 12.59 THz, ~ 7.4 times than that of silica [15]. By assuming a linear change in the Raman gain coefficient with GeO_2 concentration, we found

$$\begin{aligned}g_R(\mathrm{SiO_2-GeO_2}) = {}& (1-X_{mol\%})g_R(\mathrm{SiO_2})\\ &+X_{\mathrm{mol\%}}g_R(\mathrm{GeO_2}).\end{aligned} \tag{21}$$

Figure 2 shows the change in Raman gain spectrum for several values of GeO_2 –doping.

By using Eq. (21), we found that even a small concentration of GeO_2 (3.15mol%) shifts the peak of the Raman gain towards 12.59 THz. In fact, the peak Raman gain frequency shift, measured experimentally, is found at 13.2 THz. From Eqs. (21) and (20), the depolarized peak Raman gain for a GeO_2-doped fiber may be estimated from:

$$\begin{aligned}g_R^{peak}(\mathrm{SiO_2-GeO_2}) = {}& \frac{0.4885\times 10^{-13}}{\lambda}\\ &\times(1+6.49815X_{mol\%}),\end{aligned} \tag{22}$$

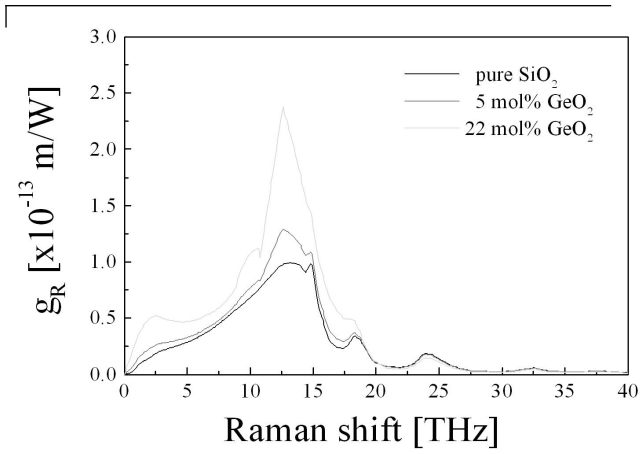

FIGURE 2. Raman gain spectrum as a function of frequency shift for several values of GeO_2 –doping.

where we have assumed that $g_R(\mathrm{GeO_2}) \approx 7.4\, g_R(\mathrm{SiO_2})$ at the peak value of the Raman gain for SiO_2, which has been reduced by a factor of two to take into account the random evolution of the polarization state of the pump and Stokes waves.

4. Five-cascades Raman Fiber Laser

Now, we use relation (19) to model a Raman fiber laser consisting of five cavities starting from a pump wavelength at 1.1μm. The output wavelength of this laser is at 1.427 μm, similar to that of Ref. 5. We assume a fiber with 22 mol% of GeO_2. The parameters of the fiber are the following: 22 mol% GeO_2, relative index difference Δn=0.032, cutoff wavelength λ_c=1.07μm, loss coefficient of 3.00 dB/km (C=3.787 dB/km μm), 1.83 dB/km (C=4.326 dB/km μm), 1.54 dB/km (C=4.398 dB/km μm), and 0.79 dB/km (C=4.559 dB/km μm) at 1.064 μm, 1.24 μm,

TABLE I. Values of the effective area, Raman gain coefficient and loss coefficient used in the simulations shown in Figs. 3-10, for the simulation and optimization of the five cascaded Raman fiber laser.

Wavelength	Effective interaction area ($\times 10^{-12}$m^2)	Raman gain ($\times 10^{-3}$W^{-1}m^{-1})	Loss coefficient ($\times 10^{-6}$ m^{-1})
1.1	8.178	9.479	595.64
1.153	9.008	8.210	493.44
1.276	9.970	7.060	404.84
1.347	11.086	6.028	375.79
1.427	12.401	4.260	307.63
1.523	-	-	244.33

1.3 μm and 1.55 μm, respectively. The values of the coefficients C of the loss values are used to correct the loss coefficient for wavelength close to the respective wavelength, assuming an inverse dependence on the fourth power of the wavelength (Rayleigh scattering), *i.e.*, $\alpha = C/\lambda^4$ [16].

In Table I, we show the calculated effective interaction areas [Eq. (3)], the Raman gains [Eq. (2)], and the absorption losses at each wavelength. Here, we calculated the mode field radii W_i using the empirical relation from Marcuse [17]:

$$W_i \approx \left(0.65 + \frac{1.619}{V^{3/2}} + \frac{2.879}{V^6}\right) a, \qquad (23)$$

where a is the core radius, and V is the normalized waveguide parameter, calculated from the relation

$$V = 2\pi\, a\, NA/\lambda. \qquad (24)$$

Here NA is the numerical aperture of the fiber, and is usually given as data from the fiber manufacturer.

Figures 3 shows the changes in the slope efficiency (P_{out}/P_{pump}) under several conditions: pump power, output reflectivity, and fiber length. Figure 3a shows that for an ideal cavity with HR mirrors of 98% and an output mirror reflectiviy of 25%, the optimum fiber length for 5W is around 32m. In Fig. 3b we assume a fixed pump power of 5W and output reflectivities of 10, 20, 30, 40, and 50%. For an output reflectivity of 10% we found an optimum length of 56.5 meters. Similar low values for the optimum cavity length were found by G. Vareille *et al.* [5], *i.e.*, 60m for HR=98% and R_{out}=10%. The difference may be due to the higher effective area used by the authors (14μm^2), and because they use the same value of effective area for all Stokes waves. Their model also predicts that the efficiency (ideal) increases as we decrease the fiber length. As can be seen in Figs. 3a and 3b, the optimum length will depend on the value of the fixed parameters, *i.e.*, pump power, output reflectivity, etc.

In addition, if we fix the cavity length we may set an optimum reflectance for a given power and/or an optimum pump power for a given output reflectivity. For ideal conditions (equal photon density for the pump and fifth Stokes, and no-losses) the maximum slope efficiency is of 77%. We can see in Figs. 3-6 that the slope efficiency does not exceed 60%, *i.e.*, 22% lower than the maximum possible under ideal conditions, due to the HR=98% and the optical losses.

The background losses (gray losses) at the gratings may be accounted for by correcting the mirror reflectivities by a factor of effective transmittance. The value of such factor will depend on the wave to be considered and the relative position of their cavity mirrors with respect to the other mirrors. Figure 4 shows the same graphs as these of Figs. 3, but now we assume that after the wave pass through any mirror, it suffers from an excess loss of 2%. This excess loss results in a reduction in the reflectance value of the mirrors. As can be seen in Fig. 4, the maximum slope efficiency does not exceed 42%, while the optimum cavity lengths are longer.

5. Comparison with Numerical Models

In Ref. 7, there is a comparison between the experimental values obtained by Grubb *et al.* [18], and those obtained through numerical simulation. The numerical simulation is done by the numerical integration of Eq. (1), without any approximation, by using collocation software for the two point boundary value problem [7]. In the experimental measurement, the laser consists of five cascades pumped at 1117nm by a diode-pumped, cladding-pumped Yb^{3+} fiber laser, and the fiber length was of 800m. Authors, in Ref. 7, use the parameters of Table II to compare with experimental results in Ref. 18. The measured threshold for an output reflectivity of 20% was of 660mW. [Here, the term output reflectivity refers to the reflectivity of the FBG output operating at the wavelength corresponding to the fifth Stokes wave (λ_5)]. Through the numerical simulation, authors in reference [7] predict a threshold power of 720mW and a slope efficiency of 42%. In fact, we found that the slope efficiency corresponding to the plot given in Fig. 9 of Ref. 7 is of 39%, and the output power predicted at 4W of pump power is of 1.29 W, while the measured value is of 1.4 W. By using our analytical model, assuming a high reflectance mirror with 99% of reflectivity and the same output reflectivity and cavity length, we found a threshold power of 640 mW and a slope efficiency of 36.5%. Figure 5a shows the comparison between the results obtained through numerical simulation in Ref. 7 and that obtained through our analytical model. The agreement between both plots is rather good, with just a 5% difference in the output power predicted by both models at 4W pump power.

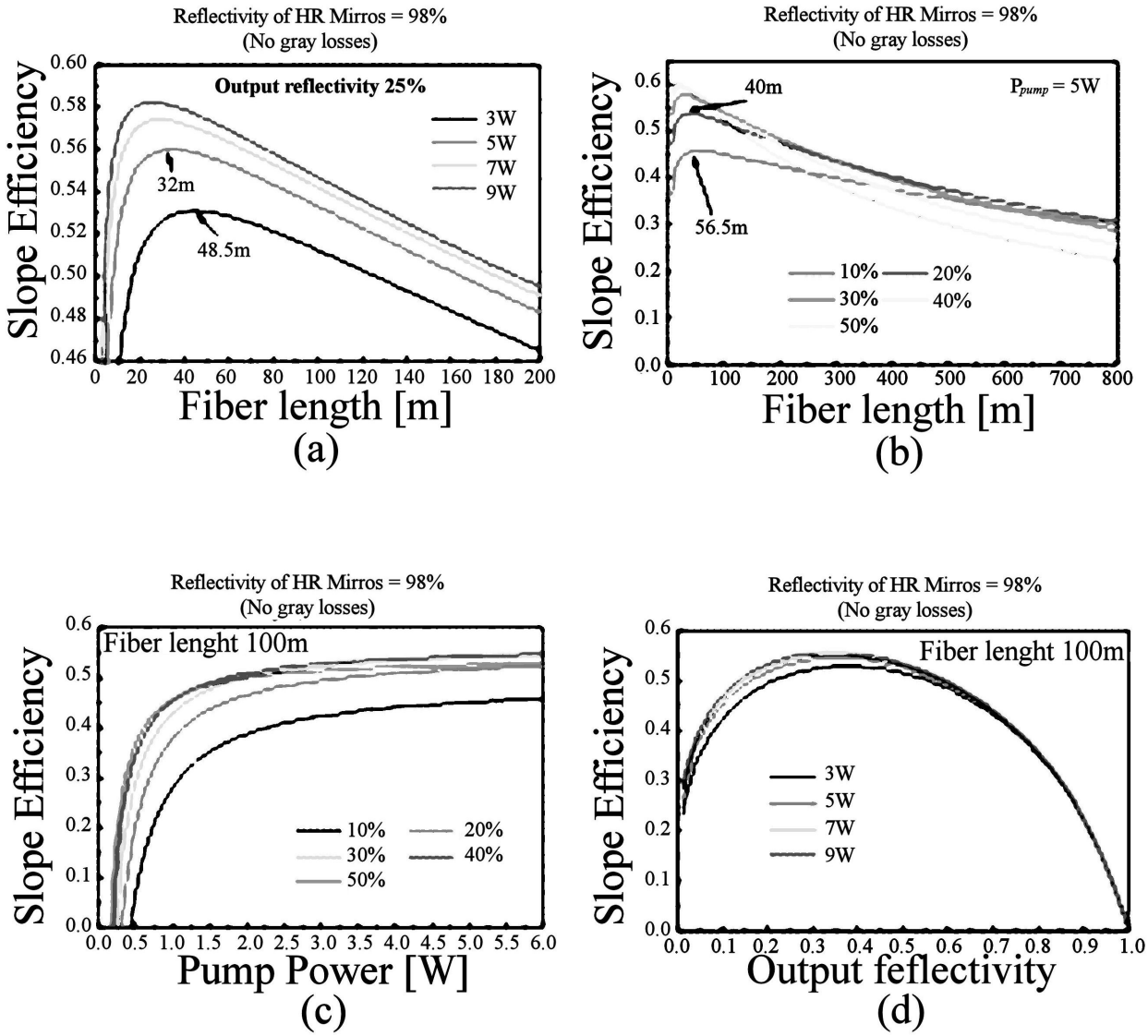

FIGURE 3. (a) Slope Efficiency as a function of cavity length, assuming an output mirror with 25% of reflectivity and several values of pump power. (HR=98%). (b) Slope Efficiency as a function of the cavity length, assuming a pump power of 5W for several values of ouput reflectivity. (HR=98%). (c) Slope Efficiency as a function of the pump power for a fixed cavity length of 100m, and several values of the output reflectivity. (d) Slope Efficiency as a function of the output reflectivity for a fixed cavity length of 100m, and several values of the pump power.

In Ref. 5 there is another numerical simulation of a six-cascades Raman laser, pumped at 1064nm. The authors assume the same effective areas for all Stokes waves and that is no detailed information about the losses coefficient at each wavelength. For a pump power of 10 W, R_{out}=10% and HR=98%, they predict an optimum cavity length of 60m, while for HR=90% the optimum length is predicted to be 170m. Figure 5b shows the optimum lengths predicted by our model, and Fig. 6 shows the conversion efficiency as a function of the pump power for both cavity lengths, assuming the same parameters of Ref. 5, showing a good agreement between the predicted lengths.

TABLE II. Parameters of the five cascaded Raman fiber lasers used in the numerical simulation of Ref. 7

Wavelength (nm)	g_R/A_{eff} $(m\cdot W)^{-1}$	αgdB/km)
1117	5.20×10^{-3}	2.12
1175	4.72×10^{-3}	1.75
1240	4.31×10^{-3}	1.54
1310	3.95×10^{-3}	1.17
1389	3.53×10^{-3}	2.63
1480	3.03×10^{-3}	0.76

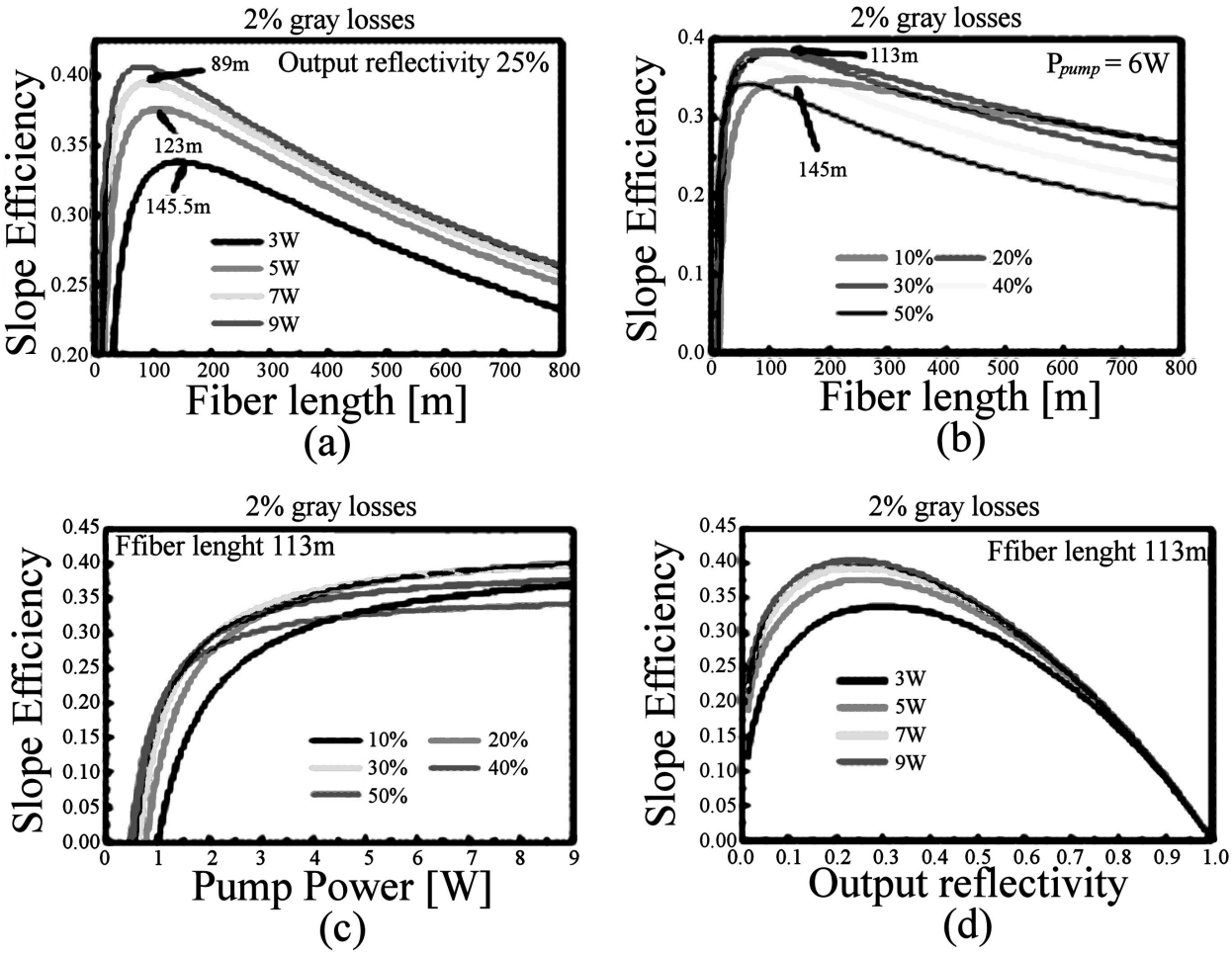

FIGURE 4. (a) Slope Efficiency as a function of the cavity length, assuming an output mirror with 25% of reflectivity and several values of pump power. (HR=99.5%). (b) Slope Efficiency as a function of cavity length, assuming apump power of 6W and several values of the output reflectivity. (HR=99.5%). (c) Slope Efficiency as a function of the pump power for a fixed cavity length of 113m, and several values of the output reflectivity. (d) Slope Efficiency as a function of the output reflectivity for a fixed cavity length of 100 m, and several values of the pump power.

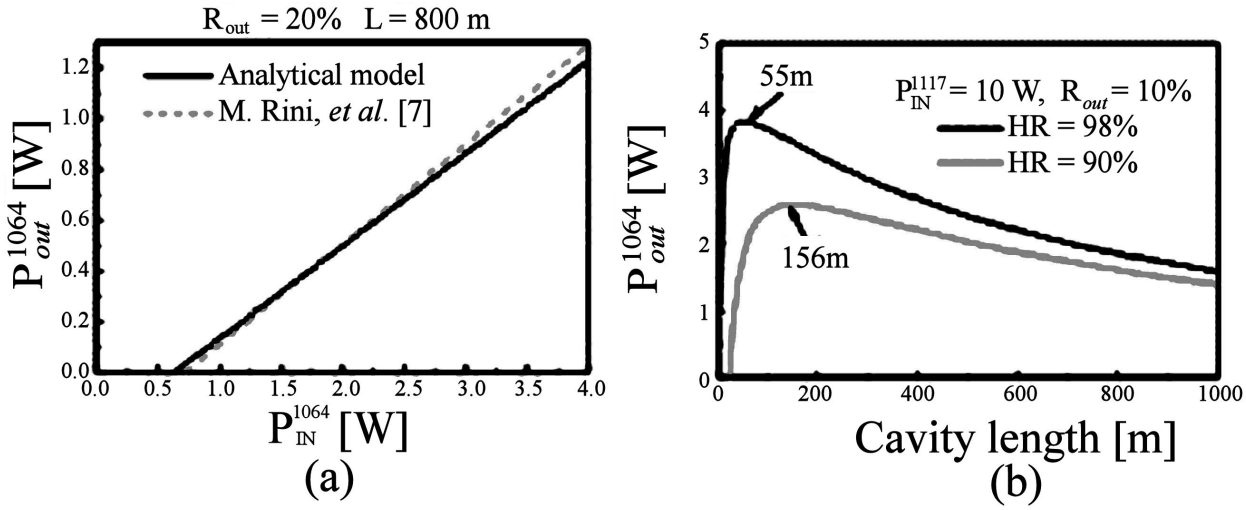

FIGURE 5. (a) Comparison between the results obtained through numerical simulation in Ref. 7 and that obtained by our analytical model. (b) Output power in a five cascades Raman fiber laser as a function of the cavity length, showing the optimum lengths. The parameters used in the simulation are the same as in Ref. 5.

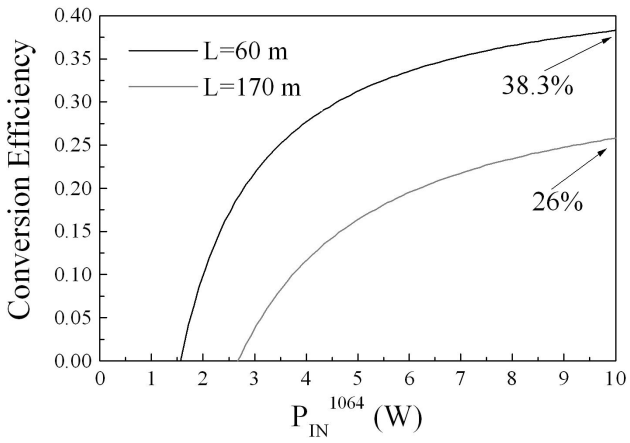

FIGURE 6. Conversion efficiency as a function of the pump power for a five cascaded Raman fiber laser. The parameters used in the simulation are the same as in Ref. 5.

6. Conclusions

We have presented an analytical approach for the analysis and design of cascaded Raman fiber lasers. The model uses the oscillation condition for the resonated Stokes waves generated inside the nested cavity Raman fiber laser, assumes that the pump is depleted in a single pass, and that the sum of the forward and backward laser Stokes waves is constant. Using these approximations, we have derived relations for the output Stokes power of a 1-, 2-, 3-, and 5-nested cavities Raman fiber laser. The formulas show the explicit dependence of the output power on the fiber parameters (length, loss, Raman gain coefficient, etc.), fiber Bragg grating reflectivity, Stokes wavelengths, and input pump power. The model was compared with numerical results obtained from literature for 5-nested cavities Raman fiber lasers showing a good agreement.

∗ Coherent laser division

1. M.D. Mermelstein *et al.*, "Six-wavelength Raman fiber laser for C+L-band Raman amplification," CLEO'02 (Long Beach, CA, 19-24 May, 2002).
2. S. B. Papernyi, V.I. Karpov, and W.R.L. Clements, "Efficient dual-wavelength Raman fiber laser," OFC'01 (Anaheim, CA, 19-22 March, 2001), paper WDD15.
3. D.I. Chang, D.S. Lim, M.Y. Jeon, K.H. Kim, and T. Park, *Electron. Lett.* **37** (2001) 740.
4. A.A. Demidov, A.N. Starodumov, X. Li, A. Martinez-Rios, and H. Po, *Opt. Lett.* **28** (2003) 1540.
5. G. Vareille, O. Audouin, and E. Desurvire, *Electron. Lett.* **34** (1998), 675.
6. W.A. Reed, W.C. Coughran, and S.G. Grubb, "Numerical modeling of cascaded CW Raman fiber amplifiers and lasers," in *Proc. Optical Fiber Communications Conf.* 1995, OFC'95, paper WD1.
7. M. Rini, I. Cristiani, and V. Degiorgio, *IEEE J. Quantum Electron.* **36** (2000) 1117.
8. M. Prabhu, N.S. Kim, L. Jianren, and K.-I. Ueda, *Opt. Review* **7** (2000) 455.
9. S. Cierullies, H. Renner, and E. Brinkmeyer, *Opt. Comm.* **217** (2003) 233.
10. J. AuYeung and A. Yariv, *JOSA* **69** (1979) 803.
11. T. Georges, "Analytic modeling of a 1.3-μm intracavity cascaded Raman amplifier", in *Proc. Optical Fiber Communications Conf.* 1995, OFC'95, paper WD2.
12. T. Nakashima, S. Seikai, and M. Nakazawa, *Opt. Lett.* **10** (1985) 420.
13. S.A. Babin, D.V. Churkin, and E.V. Podivilov, *Opt. Comm.* **226** (2003) 329.
14. S. Trillo and S. Wabnitz, *JOSA B* **9** (1992) 1061.
15. F.L. Galeener, J.C. Mikkelsen Jr., R.H. Geils, and W.J. Mosby, *Appl. Phys. Lett.* **32** (1978) 34.
16. G.P. Agrawal, *Nonlinear Fiber Optics*, second edition (Academic Press, San Diego, CA, USA, 1995).
17. A. Ghatak and K. Thyagarajan, *Introduction to Fiber Optics* (Cambridge University Press, New York, NY, USA, 1998).
18. S.G. Grubb *et al.*, "High power, 148 μm cascaded Raman laser in germanosilicate fibers," in *Proc. OAA Optical Amplifiers and Their Applications*, 1995, Paper SaA4-1, pp. 197-199.